Research Article Vol. 28, No. 9 / 27 April 2020 / Optics Express 13817
Optics EXPRESS

Determination of absorption coefficients and Urbach tail depth of ZnO below the bandgap with two-photon photoluminescence

XIAORUI WANG,[1,2] DAPENG YU,[2,3] AND SHIJIE XU[1,4]

[1]*Department of Physics, and Shenzhen Institute of Research and Innovation, The University of Hong Kong, Hong Kong, China*
[2]*Department of Physics, Southern University of Science and Technology, Shenzhen 518055, China*
[3]*yudp@sustech.edu.cn*
[4]*sjxu@hku.hk*

Abstract: In this article, we demonstrate a novel approach to determine the absorption coefficient of ZnO below the bandgap via measuring the self-absorption (SA) effect on the two-photon luminescence (TPL) spectrum of the ZnO bulk crystal rod at cryogenic temperature. Under a geometric configuration of side-excitation and front-detection, the intensities of several major spectral components of TPL spectra of ZnO can be decisively tuned by precisely varying the transmitting distance of luminescence signal, so that the absorption coefficients at different wavelengths can be determined on the basis of Beer-Lambert law. Furthermore, the peak position of donor bound exciton luminescence exhibits a unique redshift tendency with increasing the transmitting distance. Starting from the product of Lorentzian lineshape function and exponential absorption edge of Urbach tail, an analytical formula is derived to quantitatively interpret the experimental redshift characteristic with the transmitting distance. The energy depth of Urbach tail of the studied ZnO crystal is deduced to be ~13.3 meV. In principle, this new approach can be used to determine absorption coefficient of any luminescent solids as long as the SA effect happens.

© 2020 Optical Society of America under the terms of the OSA Open Access Publishing Agreement

1. Introduction

Self-absorption (SA) of luminescence is an important optical phenomenon and process which has been theoretically considered by Cowan and Dieke as early as in 1948 [1]. Besides the intensity reduction and even total disappearance of some luminescence spectral structures, it has been predicted to result in self-reversals of some spectral lines. Since it usually occurs inside luminescent body, however, the SA effect is hard to be experimentally identified and directly measured, especially in luminescent solids. As heterostructure-based semiconductor devices developed, Ettenberg and Kressel experimentally investigated the effective interfacial recombination at $Al_{0.25}Ga_{0.75}As$/GaAs and $Al_{0.5}Ga_{0.5}As$/GaAs heterojunctions [2]. They found that the interfacial recombination velocity decreases with decreasing heterojunction spacing via deducing the recombination velocity from the dependence of the minority-carrier lifetime on junction spacing in heterojunction diodes. Later, Asbeck presented a theoretical analysis of the SA effects of spontaneously emitted photons on the recombination lifetime of injected carriers in the thick active region of GaAs-GaAlAs double heterostructures, and explained the observation of Ettenberg and Kressel [3]. Moreover, from the analysis it is inferred by Asbeck that the internal quantum efficiency of radiative recombination in the heterojunction device is greater than 90%.

In fact, SA and luminescence may successively occur for many times inside a thick luminescent body so that a cascade photon recycling process could form. Recently, such photon recycling has been argued to happen efficiently in lead iodide perovskite solar cells [4] and GaInP/GaAs heterostructure solar cells [5]. In addition, the photon recycling is also taken into account in

#391534 https://doi.org/10.1364/OE.391534
Journal © 2020 Received 26 Feb 2020; revised 15 Apr 2020; accepted 15 Apr 2020; published 22 Apr 2020

Optics EXPRESS

the laser light cooling in semiconductors [6]. Nevertheless, experimental identification and demonstration studies of the SA effect in bulk semiconductors have been very few largely due to the interior happening nature of SA effect inside bulk semiconductors. Very recently, we have experimentally showed that the absence of the zero-phonon line and the first-order longitudinal optical (LO) phonon sideband in the two-photon-excited excitonic luminescence of ZnO at room temperature is indeed caused by the SA effect [7]. Compared with linear one-photon excited luminescence, the two-photon excited luminescence (TPL) is nonlinear process and may have much longer travelling distance in luminescent samples, especially in luminescent solids since the two-photon absorption usually has much smaller cross section and hence much longer penetration distance inside solids [8–10]. In terms of the importance of ZnO in both basic research and technological applications in diverse fields as a wide bandgap semiconductor [11–20], it is essential to get a better understanding of the SA effect in ZnO [7]. On the other hand, it seems an impossible task to measure absorption coefficient of a luminescent solid via photoluminescence measurement. Herein, we show that it is completely possible to obtain absorption coefficient of a luminescent solid via measuring SA effect of its photoluminescence. We present a demonstration example by investigating the SA effect on the TPL spectra of ZnO bulk crystal rod at cryogenic temperature.

2. Experimental

Figure 1 shows a schematic diagram of the experimental arrangement. The excitation light source was a mode-locked Ti:sapphire femtosecond (fs) laser with a repetition rate of 80 MHz and pulse width of 130 fs. In the TPL measurements, the laser beam was first focused by a convex lens, and then was incident on one end of a ZnO crystal rod with hexagonal shape. The focused laser beam was thus guided to enter into the rod parallel to the c-axis of the crystal rod with a length of ~30 mm and diameter of ~3 mm. The central wavelength and average power of the laser beam were controlled to be ~730 nm and 430 mW, respectively. The focusing lens can be precisely moved vertically so that the location of focusing spot of laser beam inside the crystal can be adjusted. Two collecting lenses with focal length of 10 cm and diameter of ~7 cm were placed in front of the crystal rod. The distance between the first collecting lens and the ZnO front surface was about 10 cm for effectively collecting the luminescence signal. The second colleting lens was used to

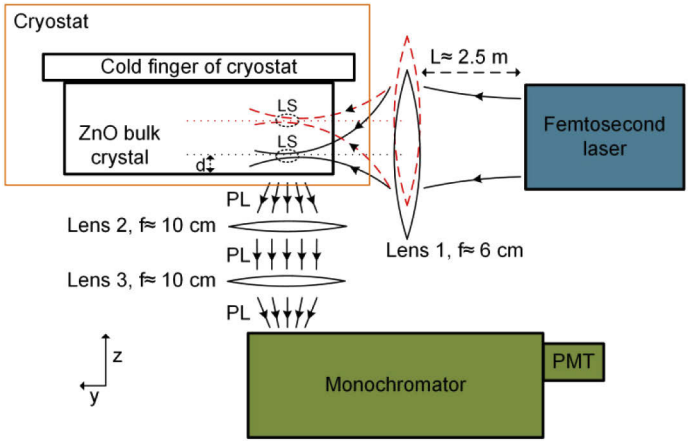

Fig. 1. A schematic diagram (not scaled) of the experimental arrangement. LS: luminescent spot; PL: photoluminescence; d: distance from the luminescence spot to the crystal front surface; f: focal length; L: spacing between the focusing lens and the laser output end. Position of the focusing lens can be precisely tuned by using a micro-stage.

Optics EXPRESS

focus the luminescence light onto the entrance slit of monochromator. Under such arrangement the distance between the laser focusing point and the collecting lens, hence the travelling distance of TPL signal from the luminescent spot to the crystal front surface can be precisely tuned. Due to the outstanding nonlinear optical nature of ZnO crystal with non-centrosymmetric wurtzite structure, the TPL signal was good enough for the precise measurements to be undertaken in the present study [7,21]. To carry out low-temperature TPL measurements, the ZnO crystal rod was attached to the cold finger of a closed cycle cryostat. The temperature of cold finger was kept at 4.15 K during the experiment.

3. Results and discussion

Figure 2(a) shows a representative TPL spectrum for a certain transmitting distance of ~110 μm, e.g., the excitation laser spot located at an interior position of the ZnO crystal rod. Three main spectral structures peaking at 375.05, 383.65 and 392.25 nm have been identified as the first-, second- and third-order longitudinal optical phonon sidebands of free excitons (FX), respectively [7]. Their corresponding photon energies were 3.306, 3.232 and 3.161 eV, denoted as FX-LO, FX-2LO and FX-3LO, respectively. Just for comparison's sake, Fig. 2(b) shows a one-photon luminescence (OPL) spectrum of the ZnO rod at cryogenic temperature with a 325 nm CW laser incident on the front surface of the rod. Utilizing this normal arrangement, the OPL signal was only produced from the skin layer of the rod due to the high absorption coefficient and hence extremely shallow absorption depth (tens of nm) of the 325 nm laser. In other words, The OPL signal suffered from a negligible SA effect. Clearly, the OPL spectrum in Fig. 2(b) has more spectral structures, e.g., 367.59, 374.80, 383.37 and 391.91 nm spectral components which have been identified as the FX line and its three-orders LO phonon sidebands [7]. The most dominant component was the neutral donor bound exciton (DX) line at 369.36 nm in the OPL spectrum. Its first- and second-order LO sidebands (denoted as DX-LO and DX-2LO) were also identified to have the peak wavelengths of 377.15 and 385.72 nm, respectively [7]. In sharp contrast to the OPL spectrum, the TPL spectrum was dominated by FX-LO rather than DX. It has been previously established that the elimination of DX and FX lines in the TPL spectrum is caused by the SA effect [7]. Moreover, the SA effect has been rigorously proven to strictly obey the well-known Beer-Lambert law [7]. Here we focus on how the intensity reduction of various spectral lines is controlled by the law.

Shown in the left upper inset picture is photography of the ZnO rod under the excitation of 780 nm fs laser. The green color luminescence was from trace Cu ions in ZnO crystal [22–25]. Note that the green luminescent spot with the shape of spindle looks larger than the actual focusing point probably due to the scattering of the green luminescence in the crystal [26]. By adjusting the focusing lens position to increase the distance from the luminescent spot to the crystal front surface, e.g., by shifting the focusing lens along z-direction, FX-2LO can become a leading structure in the TPL spectrum for the distance >250 μm, as shown in Fig. 2(a). Obviously, the relative intensities of various spectral structures can be tuned via changing the travelling distance of TPL signal. Actually this distance is the experiencing distance of SA effect. Such an experimental arrangement hence offers us an opportunity to conduct an in-depth investigation of the SA effect.

Figure 3 shows the measured TPL spectra for different distances from 0 to 600 μm. In the case of $d = 0$, the leading structure at 370.6 nm was DX line. As the distance increases, the intensities of all spectral structures including DX line, FX-LO, FX-2LO become less. Meanwhile, the relative intensity of DX line decreases with respect to FX-LO and even FX-2LO. When $d = 110$ μm, the DX line became almost unobservable, and the FX-LO structure was dominant in the spectrum. With further increasing the distance, the FX-LO intensity declined quickly, and the FX-2LO structure eventually developed as the leading component as shown in Fig. 3(b).

Optics EXPRESS

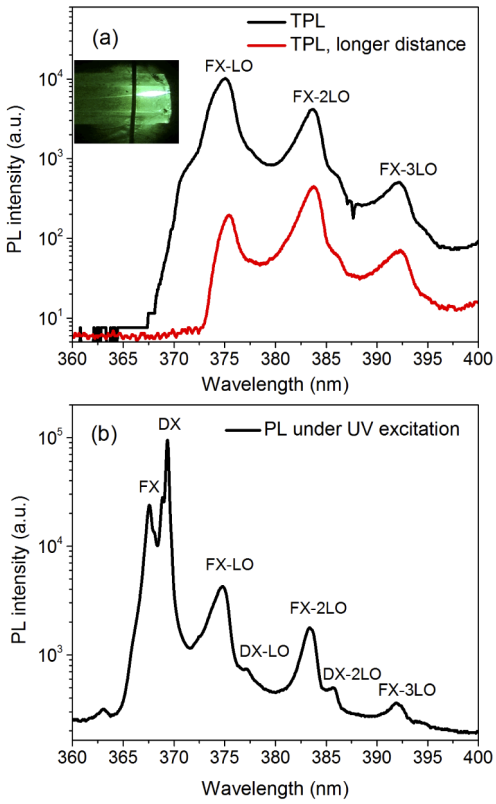

Fig. 2. PL spectra of the ZnO crystal rod measured at 4.15 K. (a) Measured TPL spectra for two different distances from the luminescent spot inside the crystal to the crystal front surface. The distance was ~110 μm for top one, while >250 μm for bottom one. The inset is a TPL photograph of the crystal rod emitting the green light under the side-end excitation of 780 nm fs laser. (b) Measured one-photon excited PL spectrum of the crystal rod under the front-surface excitation of 325 nm UV laser.

Since the SA effect is also strictly controlled by the Beer-Lambert law [7], it is possible for one to obtain absorption information from the measured intensity evolution of TPL spectral structures with the distance. Figures 4(a)-(c) show the experimental luminescence peak intensities (solid squares) of DX, FX-LO and FX-2LO versus the distance, respectively. On the basis of Beer-Lambert law, e.g., $I_d = I_0 \exp(-\alpha d)$, in which I_d, I_0, and α refer to the TPL intensity at distance of d, the initial intensity at $d = 0$, and absorption coefficient, respectively, the measured TPL intensity evolution curves may be represented as exponential decay curves. As shown in Fig. 4, good agreement between experiment and theory is achieved for all major spectral components including DX, FX-LO and FX-2LO. The experimental peak intensity fluctuations in Figs. 4(b)–4(c) in the range of 140-280 μm are likely caused by the local roughness on the ZnO side entrance-surface. When the laser beam was scanned over this rough area, the effective intensity of laser beam entering inside the crystal fluctuates and hence the TPL signal varies. The absorption coefficients adopted in the fitting curves (solid lines) in Figs. 4(a)–4(c) were 298.4, 109.6 and 62.8 cm^{-1}, respectively, for the spectral components of DX, FX-LO and FX-2LO. In fact, all absorption coefficients below the bandgap can be principally obtained using such approach. The deduced absorption coefficients of 298.4, 109.6 and 62.8 cm^{-1} at ~370.6, 375.05 and 383.65 nm are consistent with available experimental data in literature [27–29]. Besides, it can be found that the intensity decline rates of various luminescence structures are different

Optics EXPRESS

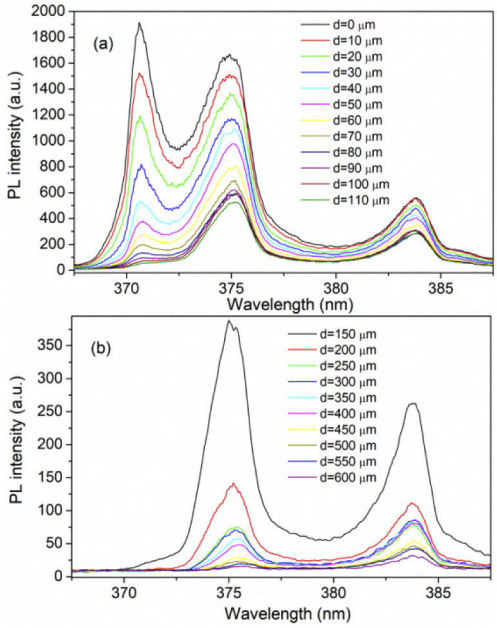

Fig. 3. Measured TPL spectra for various distances from the luminescent spot to the crystal front surface. (a) The leading position of DX line is gradually replaced by FX-LO as the distance increases from zero. (b) As the distance is further increased, FX-2LO structure becomes dominant peak in the spectrum.

because the absorption coefficient depends strongly on wavelength. In Fig. 4(d), the experimental data and corresponding fitting curves are depicted together for comparison. Evidently, the intensity decline rate becomes smaller as the wavelength increases. If a ratio is defined as $R_d = I_d / I_0$, it is easy to conclude that $R_d = \exp(-\Delta\alpha d)$, where $\Delta\alpha$ is absorption coefficient difference between two different wavelengths.

In addition to the peak intensity decline, the peak position of DX line exhibits a distinctive redshift, especially when the distance is increased in the beginning small range of 0-40 μm, as can be seen in Fig. 5. Such redshift tendency may be interpreted as the modulation effect of an exponential absorption edge on the Lorentzian lineshape of DX line. Usually, the lineshape of bound excitonic optical transitions in binary semiconductors can be treated as Lorentzian profile [30]:

$$L_{(\upsilon)} = A\frac{1}{\pi}\frac{\Gamma/2}{(\upsilon-\upsilon_0)^2+(\Gamma/2)^2}, \tag{1}$$

where υ, υ_0, Γ and A refer to frequency, central frequency, full width at half maximum (FWHM) and a constant, respectively. Here υ is rescaled by $\upsilon = h\upsilon_i / eV$, where h is the Planck constant and υ_i is the original frequency in unit of Hz. Γ is in unit of eV. The exponential absorption edge of Urbach tail induced by defects states below bandgap can be expressed as

$$\alpha_{(\upsilon)} = \alpha_0 \exp[(\upsilon-\upsilon_0)/E_0], \tag{2}$$

where α_0 is the absorption coefficient at υ_0, and E_0 is in unit of eV reflecting the exponential edge depth [31–33]. After transmitting a distance of z with SA effect, the spectral lineshape of DX line shall take an expression

$$F_{(\upsilon,z)} = L_{(\upsilon)} \exp[-\alpha_{(\upsilon)} z]. \tag{3}$$

Optics EXPRESS

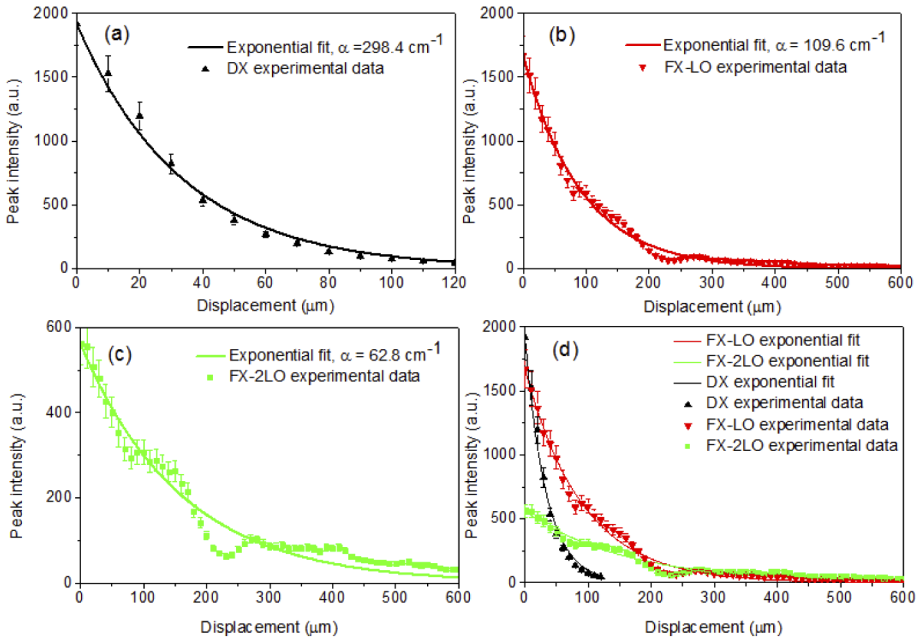

Fig. 4. Experimental peak intensities (solid squares) decline vs. the displacement. Solid curves represent the fitting curves with Beer-Lambert law for DX (a), FX-LO (b) and FX-2LO (c), respectively. (d) The peak intensity reduction tendencies of the three structures are shown together for comparison. The intensity decline rate decreases as the wavelength increases because the absorption coefficient difference becomes smaller. Experimental errors are also provided.

By solving $\partial F_{(\upsilon,z)} \big/ \partial \upsilon = 0$, one can determine the spectral peak frequency υ which is dependent on z.

For $|\upsilon - \upsilon_0| << E_0$, $\exp[(\upsilon - \upsilon_0)/E_0]$ at right hand side of Eq. (2) may be approximated as $[1 + (\upsilon - \upsilon_0)/E_0]$ under its first-order Taylor approximation. Then an approximate solution of Eq. (3) may be obtained as

$$\upsilon = (-q/2 + r)^{1/3} + (-q/2 - r)^{1/3} + (\upsilon_0 - E_0/3), \tag{4}$$

where

$$r = [(q/2)^2 + (p/3)^3]^{1/2}, \tag{5}$$

and

$$q = E_0\Gamma^2 \Big/ 6 + 2E_0^3 \Big/ 27 - 2E_0^3 \Big/ 3\alpha_0 z, \tag{6}$$

$$p = \Gamma^2 \Big/ 4 + 2E_0^2 \Big/ \alpha_0 z - E_0^2 \Big/ 3. \tag{7}$$

The solid line in Fig. 5(a) represents a fitting curve to the experimental data with Eq. (4). The adopted values of υ_0 and Γ in fitting were 3.356 and 0.011 eV, respectively, whereas the values of α_0 and E_0 were adopted to be 1553.1 cm^{-1} and 0.0133 eV, respectively. Good agreement between the fitting curve and the experimental data is achieved. Therefore, the observed distinctive redshift of peak position of DX line indeed stems from the SA effect. If the fitting curve is plotted in an enlarged range of displacement, the Urbach tail depth E_0 may be found, as shown in Fig. 5(b). In the case of ZnO bulk rod studied here, E_0 was found to be ~13.3 meV.

Optics EXPRESS

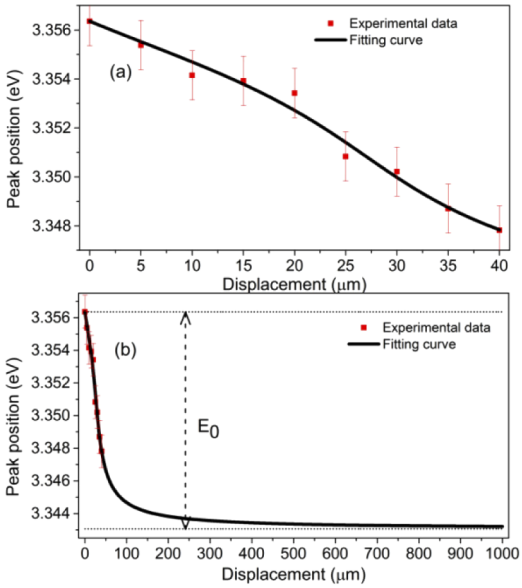

Fig. 5. (a) Experimental peak positions (solid squares) of DX line vs. the displacement, and a fitting curve with Eq. (4) described in text. (b) Experimental data and fitting curve in an enlarged range of displacement. The exponential absorption edge width may be found in such a large displacement scale. Experimental errors are also given.

Possible experimental errors were analyzed below. Even the displacement of the focusing lens was taken as the variation of distance between the luminescent spot inside the crystal and the crystal front surface, an error of 2.4% was estimated. If without considering the SA effect, the maximum 600 μm displacement of the luminescence spot itself may result in an estimated 0.56% variation in TPL intensity.

4. Conclusions

In conclusion, the SA effect on the major spectral structures of two-photon luminescence spectrum of ZnO crystal at cryogenic temperature is investigated under the geometric configuration of side-excitation and front-detection using near-infrared fs laser as the excitation light source. By varying the transmitting distance of luminescence signal inside the crystal, the intensities of the major spectral structures including DX, FX-LO and FX-2LO can be finely tuned so that the absorption coefficients of ZnO below bandgap are determined. In addition, the observed distinctive redshift of peak position of DX line with respect to the transmitting distance is quantitatively interpreted on the basis of the product of Lorentzian lineshape function and exponential absorption edge of Urbach tail. Under the first-order approximation, an analytical formula is found for the characteristic redshift of DX line with increasing the distance of SA effect. The study also leads to the determination of energetic width of Urbach tail of the studied ZnO crystal. More importantly, the conclusions of this study are generally true for luminescent solids.

Funding

Science, Technology and Innovation Commission of Shenzhen Municipality (JCJY20180508163404043, JCYJ20170818141709893); Research Grants Council, University Grants Committee (HKU703612P); National Natural Science Foundation of China (11374247).

Optics EXPRESS

Disclosures

The authors declare no conflicts of interest.

References

1. R. D. Cowan and G. H. Dieke, "Self-absorption of spectrum lines," Rev. Mod. Phys. **20**(2), 418–455 (1948).
2. M. Ettenberg and H. Kressel, "Interfacial recombination at (AlGa) As/GaAs heterojunction structures," J. Appl. Phys. **47**(4), 1538–1544 (1976).
3. P. Asbeck, "Self-absorption effects on the radiative lifetime in GaAs-GaAlAs double heterostructures," J. Appl. Phys. **48**(2), 820–822 (1977).
4. L. M. Pazos-Outón, M. Szumilo, R. Lamboll, J. M. Richter, M. Crespo-Quesada, M. Abdi-Jalebi, H. J. Beeson, M. Vrućinić, M. Alsari, H. J. Snaith, B. Ehrler, R. H. Friend, and F. Deschler, "Photon recycling in lead iodide perovskite solar cells," Science **351**(6280), 1430–1433 (2016).
5. Z. Su, S. Xu, X. Wang, J. Ning, R. Wang, S. Lu, J. Dong, and H. Yang, "Effective photon recycling and super long lived minority carriers in GaInP/GaAs heterostructure solar cell: a time-resolved optical study," IEEE J. Photovoltaics **8**(3), 820–824 (2018).
6. M. Sheik-Bahae and R. I. Epstein, "Can laser light cool semiconductors?" Phys. Rev. Lett. **92**(24), 247403 (2004).
7. H. Ye, Z. Su, F. Tang, C. Zheng, G. Chen, J. Wang, and S. Xu, "Extinction of the zero-phonon line and the first-order phonon sideband in excitonic luminescence of ZnO at room temperature: the self-absorption effect," Sci. Bull. **62**(22), 1525–1529 (2017).
8. See for example, in *Topics in Fluorescence Spectroscopy: Nonlinear and Two-Photon-Induced Fluorescence* (Kluwer, New York 2002), Vol. 5, J. R. Lakowicz, Ed.
9. W. Denk, J. H. Strickler, and W. W. Webb, "Two-photon laser scanning fluorescence Microscopy," Science **248**(4951), 73–76 (1990).
10. K. Wei, Z. Xu, R. Chen, X. Zheng, X. Cheng, and T. Jiang, "Temperature-dependent excitonic photoluminescence excited by two-photon absorption in perovskite $CsPbBr_3$ quantum dots," Opt. Lett. **41**(16), 3821–3824 (2016).
11. See for example, a critical review and reference therein, C. Klingshirn, J. Fallert, H. Zhou, J. Sartor, C. Thiele, F. Maier-Flaig, D. Schneider, and H. Kalt, "65 years of ZnO research–old and very recent results," Phys. Status Solidi B **247**(6), 1424–1447 (2010).
12. Z. L. Wang and J. Song, "Piezoelectric nanogenerators based on zinc oxide nanowire arrays," Science **312**(5771), 242–246 (2006).
13. C. Battaglia, J. Escarre, K. Soderstrom, M. Charriere, M. Despeisse, F.-J. Haug, and C. Ballif, "Nanomoulding of transparent zinc oxide electrodes for efficient light trapping in solar cells," Nat. Photonics **5**(9), 535–538 (2011).
14. O. Jamadi, F. Reveret, P. Disseix, F. Medard, J. Leymarie, A. Moreau, D. Solnyshkov, C. Deparis, M. Leroux, E. Cambril, S. Bouchoule, J. Zuniga-Perez, and G. Malpuech, "Edge-emitting polariton laser and amplifier based on a ZnO waveguide," Light: Sci. Appl. **7**(1), 82 (2018).
15. G. Vampa, T. J. Hammond, M. Taucer, X. Ding, X. Ropagnol, T. Ozaki, S. Delprat, M. Chaker, N. Thiré, B. E. Schmidt, F. Légaré, D. D. Klug, A. Yu Naumov, D. M. Villeneuve, A. Staudte, and P. B. Corkum, "Strong-field optoelectronics in solids," Nat. Photonics **12**(8), 465–468 (2018).
16. D. You, C. Xu, J. Zhao, F. Qin, W. Zhang, R. Wang, Z. Shi, and Q. Cui, "Single-crystal ZnO/AlN core/shell nanowires for ultraviolet emission and dual-color ultraviolet photodetection," Adv. Opt. Mater. **7**(6), 1801522 (2019).
17. D. C. Look, B. Claflin, Y. I. Alivov, and S. J. Park, "The future of ZnO light emitters," Phys. Status Solidi A **201**(10), 2203–2212 (2004).
18. Ü. Özgür, Y. I. Alivov, C. Liu, A. Teke, M. A. Reshchikov, S. Doğan, V. Avrutin, S.-J. Cho, and H. Morkoç, "A comprehensive review of ZnO materials and devices," J. Appl. Phys. **98**(4), 041301 (2005).
19. A. Kołodziejczak-Radzimska and T. Jesionowski, "Zinc oxide-from synthesis to application: a review," Materials **7**(4), 2833–2881 (2014).
20. M. A. Borysiewicz, "ZnO as a Functional Material, a Review," Crystals **9**(10), 505 (2019).
21. D. C. Dai, S. J. Xu, S. L. Shi, M. H. Xie, and C. M. Che, "Efficient multiphoton-absorption-induced luminescence in single-crystalline ZnO at room temperature," Opt. Lett. **30**(24), 3377–3379 (2005).
22. R. Dingle, "Luminescent transitions associated with divalent copper impurities and the green emission from semiconducting zinc oxide," Phys. Rev. Lett. **23**(11), 579–581 (1969).
23. S. L. Shi, G. Q. Li, S. J. Xu, Y. Zhao, and G. H. Chen, "Green luminescence band in ZnO: fine structures, electron-phonon coupling, and temperature effect," J. Phys. Chem. B **110**(21), 10475–10478 (2006).
24. H. Ye, Z. Su, F. Tang, M. Wang, G. Chen, J. Wang, and S. Xu, "Excitation dependent phosphorous property and new model of the structured green luminescence in ZnO," Sci. Rep. **7**(1), 41460 (2017).
25. H. Ye, Z. Su, F. Tang, Y. Bao, X. Lao, G. Chen, J. Wang, and S. Xu, "Probing defects in ZnO by persistent phosphorescence," Opto-Electronic Adv. **1**, 180011 (2018).
26. X. Wang, H. Ye, Z. Su, D. Yu, and S. Xu, "Observation of two-times self-focusing of femtosecond laser beam in ZnO crystal by two-photon luminescence," Sci. Bull. **63**(21), 1392–1396 (2018).
27. V. Srikant and D. R. Clarke, "Optical absorption edge of ZnO thin films: the effect of substrate," J. Appl. Phys. **81**(9), 6357–6364 (1997).

Optics EXPRESS

28. G. H. Jensen and T. Skettrup, "Absorption edge and urbach's rule in ZnO," Phys. Status Solidi B **60**(1), 169–173 (1973).
29. Y. Natsume, H. Sakata, and T. Hirayama, "Low-temperature electrical conductivity and optical absorption edge of ZnO films prepared by chemical vapour deposition," Phys. Status Solidi A **148**(2), 485–495 (1995).
30. E. F. Schubert, E. O. Göbel, Y. Horikoshi, K. Ploog, and H. J. Queisser, "Alloy broadening in photoluminescence spectra of Al $_x$ Ga $_{1-x}$ As," Phys. Rev. B **30**(2), 813–820 (1984).
31. R. C. Rai, "Analysis of the Urbach tails in absorption spectra of undoped ZnO thin films," J. Appl. Phys. **113**(15), 153508 (2013).
32. J. I. Pankove, "Absorption edge of impure gallium arsenide," Phys. Rev. **140**(6A), A2059–A2065 (1965).
33. G. D. Cody, T. Tiedje, B. Abeles, B. Brooks, and Y. Goldstein, "Disorder and the optical-absorption edge of hydrogenated amorphous silicon," Phys. Rev. Lett. **47**(20), 1480–1483 (1981).

147.8.230.85 {ts '2020-10-08 00:13:31'}